This is a repository copy of *Eutectic superalloys for laser powder bed fusion*.

White Rose Research Online URL for this paper:
https://eprints.whiterose.ac.uk/221825/

Version: Accepted Version

Proceedings Paper:

Christofidou, K.A. orcid.org/0000-0002-8064-5874, Wilson, A.S., Markanday, J.F.S. et al. (6 more authors) (2024) Eutectic superalloys for laser powder bed fusion. In: Superalloys 2024: Proceedings of the 15th International Symposium on Superalloys. 15th International Symposium on Superalloys, 08-12 Sep 2024, Champion, Pennsylvania, USA. The Minerals, Metals & Materials Series . Springer Nature Switzerland , pp. 860-870. ISBN 9783031639364

https://doi.org/10.1007/978-3-031-63937-1_80

© 2024 The Authors. Except as otherwise noted, this author-accepted version of a journal article published in Superalloys 2024: Proceedings of the 15th International Symposium on Superalloys is made available via the University of Sheffield Research Publications and Copyright Policy under the terms of the Creative Commons Attribution 4.0 International License (CC-BY 4.0), which permits unrestricted use, distribution and reproduction in any medium, provided the original work is properly cited. To view a copy of this licence, visit http://creativecommons.org/licenses/by/4.0/

Reuse
This article is distributed under the terms of the Creative Commons Attribution (CC BY) licence. This licence allows you to distribute, remix, tweak, and build upon the work, even commercially, as long as you credit the authors for the original work. More information and the full terms of the licence here: https://creativecommons.org/licenses/

Takedown
If you consider content in White Rose Research Online to be in breach of UK law, please notify us by emailing eprints@whiterose.ac.uk including the URL of the record and the reason for the withdrawal request.

eprints@whiterose.ac.uk
https://eprints.whiterose.ac.uk/

Eutectic Superalloys for Laser Powder Bed Fusion

K. A. Christofidou[1*], A. S. Wilson[2], J. F. S. Markanday[2], E. J. Pickering[3] N. L. Church[2], J. R. Miller[2], N. G. Jones[2], C. N. Jones[4] & H. J. Stone[2]

[1] University of Sheffield, Department of Materials Science and Engineering, Mappin St, Sheffield City Centre, Sheffield S1 3JD, UK

[2] University of Cambridge, Department of Materials Science & Metallurgy, 27 Charles Babbage Road, Cambridge, CB3 0FS, UK

[3] The University of Manchester, Department of Materials Science and Engineering, Oxford Road, Manchester, M13 9PL

[4] Rolls-Royce plc, PO Box 31, Derby, DE24 8BJ, UK

* Corresponding author (K.A.C) email: k.christofidou@sheffield.ac.uk

Email Addresses:
A.S. Wilson: asw33@cantab.ac.uk
J.F.S. Markanday: jfsm2@cam.ac.uk
E.J. Pickering: ed.pickering@manchester.ac.uk
N.L. Church: nc457@cam.ac.uk
J.R. Miller: jm2058@cam.ac.uk
N.G. Jones: ngj22@cam.ac.uk
C.N. Jones: c.n.jones@virginmedia.com
H.J. Stone: hjs1002@cam.ac.uk

Abstract (150-250 words)

Due to the small freezing range of eutectic alloys, the Cotac-type alloys might be viable alternatives to conventional Ni-based superalloys when processed through additive manufacturing. Laser-pass assessment reveals that both Cotac-74 and Cotac-744 display improved cracking resistance when compared to the conventional Ni-based superalloy CM247LC. During laser powder bed fusion Cotac-74 displayed the highest cracking resistance, with no microcracking detected in the as-built or heat-treated microstructure. The promising results presented for Cotac-74 highlight the possible use of this alloy for the additive manufacturing of high-temperature aerospace components.

Keywords: nickel alloys; laser methods; electron microscopy; *in-situ* composites; additive manufacturing; other

Introduction

Laser powder bed fusion (LPBF) is of tremendous interest to the aerospace industry, offering opportunities for the production of geometrically complex components that may deliver improved in-service performance. However, whilst low γ' (<30 vol.%) and γ'' superalloys can be routinely and reliably manufactured using LPBF, significant challenges remain in the LPBF processing of high γ' alloys [1, 2]. In particular, solidification and liquation cracking frequently occur during fabrication, while higher γ' alloys may also experience strain-age cracking when exposed to high temperatures in post-processing operations [3, 4]. The strain-age cracking susceptibility of high γ' superalloys is believed to be a result of large residual stresses developing within the material linked to the precipitation of the γ' phase. Consequently, to improve the processability of these alloys, three key research strategies form the focus of the majority of the open literature; the optimisation of process parameters during fabrication, the chemical modification of the alloys, and the design of novel superalloy compositions that are intrinsically resistant to both hot and strain-age cracking [4-8].

In this study, an alternative strategy is considered, namely the investigation of alloy systems that exploit eutectic invariant reactions as a means of improving the cracking susceptibility of high γ' superalloys without compromising the alloy performance. It has been reported that controlling the freezing range can reduce, or in some instances eliminate, solidification cracking [9-11]. As such, eutectic alloys, which possess an intrinsically narrow freezing range, might enable the LPBF of alloys with high fractions of γ'. The systems Cotac-74 and Cotac-744 are eutectic Ni-based superalloys containing γ, γ' and MC-type carbides that were developed by ONERA during the 1970s to be used as directionally solidified composites for turbine blades and nozzle guide vanes [12] [13]. These alloys offered a good combination of mechanical performance and satisfactory oxidation resistance at temperatures in excess of 900 °C. The microstructures of these *in-situ* composites were based around the γ–γ'–MC eutectic, with carbide fibres running through the microstructure along the solidification direction.

However, they did not achieve commercialisation due to the uneconomic furnace withdrawal rates required to maintain a planar front during solidification.

To date, there has been no research into the additive manufacturing of either Cotac-74 or Cotac-744, or indeed any other Ni-based eutectic alloys. The work herein, aims to present an initial investigation of the amenability of the Cotac-74 and Cotac-744 alloys to LPBF, focusing primarily on the cracking susceptibility of the alloys. Comparisons are made to the behaviour of CM247LC. Particular attention has been given to the microstructural evolution of the alloys during processing and post-built heat treatment.

Experimental Methods

The nominal compositions of the alloys investigated in this study are given in Table 1 [12, 14].

Table 1 – Compositions of the alloys used in this study in wt %. The balance in Ni in each case.

Alloy	Al	Co	Cr	Hf	Nb	Mo	Ta	Ti	W	C	B	Zr
Cotac-74	**4**	**20**	**10**	**-**	**4.9**	**-**	**-**	**-**	**10**	**0.6**	**-**	**-**
Cotac-744	**6**	**10**	**4**	**-**	**3.8**	**2**	**-**	**-**	**10**	**0.47**	**-**	**-**
CM247LC	**5.6**	**9.2**	**8.1**	**1.4**	**-**	**0.5**	**3.2**	**0.7**	**9.5**	**0.07**	**0.015**	**0.015**

The alloy samples investigated in this study were produced via two routes; (i) vacuum arc-melting and (ii) LPBF. This permitted analysis and comparison of the microstructure produced by the two routes as well as an initial assessment of the propensity to cracking during surface laser passes.

The surface laser passes were carried out using the bead-on-plate method on arc melted ingots to determine the cracking tendency, similar to the bead-on-plate test carried out by Zhou *et al.* [13]. For these tests, a laser was rastered across a flat surface that had been ground to a 1200 SiC grit finish. Conventionally cast CM247LC was included in this testing to provide a benchmark for interpretation of the results. Three sets of laser-passes were performed on each alloy with energy densities per unit area of 2.25 J/mm^2, 3.17 J/mm^2 and 4.04 J/mm^2, henceforth referred to as low, medium and high respectively.

The assessment of cracking susceptibility was performed qualitatively from optical and electron micrographs of the laser-scanned surface of the samples (shown as binary threshold insets in Figure 1). The samples were subsequently cut in cross-section, mounted and prepared for microscopy following standard metallographic preparation techniques culminating in a final polishing step with 0.04 µm colloidal silica solution. This allowed the analysis of the laser heat-affected zone (HAZ) with depth into the ingot surface to be assessed. Scanning electron microscopy (SEM) was performed using a Zeiss GeminiSEM 300 fitted with an Oxford Instruments X-MaxN 50 energy dispersive X-ray (EDX) detector for compositional analysis of the microstructural features. Where required, processing the sample images was achieved using the open-source ImageJ software.

LPBF samples were built using custom powder with a powder size of 15 µm - 45 µm. Samples manufactured using LPBF were supplied by Rolls-Royce plc. As no process optimisation was explored for this work, the lowest energy density of 2.25 J/mm^2 was chosen as appropriate based on the laser passes investigated coupled with a bilinear raster scan strategy to produce rectilinear columns. No additional hot isostatic pressing treatments were applied to the as-built samples. However, in addition to microstructural evaluations of material in the as-cast and as-built states, samples were also heat treated and aged following the guidelines reported by Khan *et al.*[12] and modified based on differential scanning calorimetry results to ensure super-solvus solution heat treatments were utilised. All samples were removed from the baseplate using electro-discharge machining prior to heat treatments. Cotac-74 samples were homogenised at 1125 ˚C for 1 hour and aged for 16 hours at 760 ˚C, whereas Cotac-744 samples were homogenised at 1260 ˚C for 1 hour and aged for 16 hours at 850 ˚C. For both alloys, air cooling to room temperature was used between each heat treatment step. All samples were heat treated in Ar-backfilled quartz ampoules to limit oxidation effects on the samples. Henceforth the heat treatments will be referred to as "as-built" for no heat treatment and "solution-aged" for the fully heat-treated condition.

Differential scanning calorimetry (DSC) was performed using a Netzsch 404 calorimeter on disc-shaped samples of approximately 5 mm diameter and 1 mm thickness of each alloy. Transition temperatures were obtained from the deviations from baseline of the first derivative curves. Using this method, the γ' solvus and the material solidus temperatures were extracted from the heating data whilst the liquidus temperature was determined from the cooling data.

X-ray diffraction (XRD) data were collected from Cotac-74 and Cotac-744 samples using a Bruker D8 DAVINCI diffractometer fitted with a CuKα source and a Ni filter. Data were acquired over a 2θ range of 20 to 100° with a step size of 0.05° and a dwell time of 3 seconds. The diffraction data were analysed using full-pattern Pawley refinements in Topas-Academic**.**

Samples for transmission electron microscopy (TEM) were extracted from selected regions of interest using focused ion beam milling (FIB) and were spot attached to a TEM grid. Electron micrographs and selected-area diffraction patterns (SADP) were acquired from the FIB samples using an FEI™ Tecnai Talos TEM operated at 200 kV. The scanning transmission electron microscopy (STEM) mode was used to perform EDX for compositional analysis using a Bruker XFlash detector in the same instrument.

Results and Discussion

3.1 Laser-pass Assessment

The viability of the Cotac-74 and Cotac-744 for LPBF was determined through laser-pass assessments on polished surfaces of the as-cast samples. Figure 1 shows cross-sectional micrographs through the laser passes for Cotac-74 and Cotac-744 as well as CM247LC, which was used as a benchmark material to assess the viability of the methodology utilised. In addition, insets for each condition in Figure 1 show binary thresholded images of a larger area of the laser pass surface, qualitatively highlighting the crack density for each material in each condition. As expected, CM247LC exhibited cracking in all energy densities used, with an increase in energy density leading to higher cracking susceptibility. In contrast, both alloys Cotac-74 and Cotac-744 show reduced cracking densities. Cotac-744 showed no cracking at low energy density, with some cracking being observed in the medium and high energy densities, albeit this appeared to be of reduced severity when compared to CM247LC. Cotac-74 was found to exhibit no visible cracking in any of the conditions assessed, consistent with this material comprising a lower γ' fraction compared to Cotac-744.

In addition to the cracking susceptibility, the micrographs in Figure 1 also show the microstructural changes of the material within the heat affected zone of the laser pass compared to the as-cast structure. All samples show the development of a heat affected region where a typical epitaxial structure with high levels of intragranular misorientation can be observed. Of particular note is the dissolution of the finer carbide phases within the laser pass region in

Cotac-74 and Cotac-744, suggesting that optimisation of the microstructure of these materials could indeed be possible in LPBF.

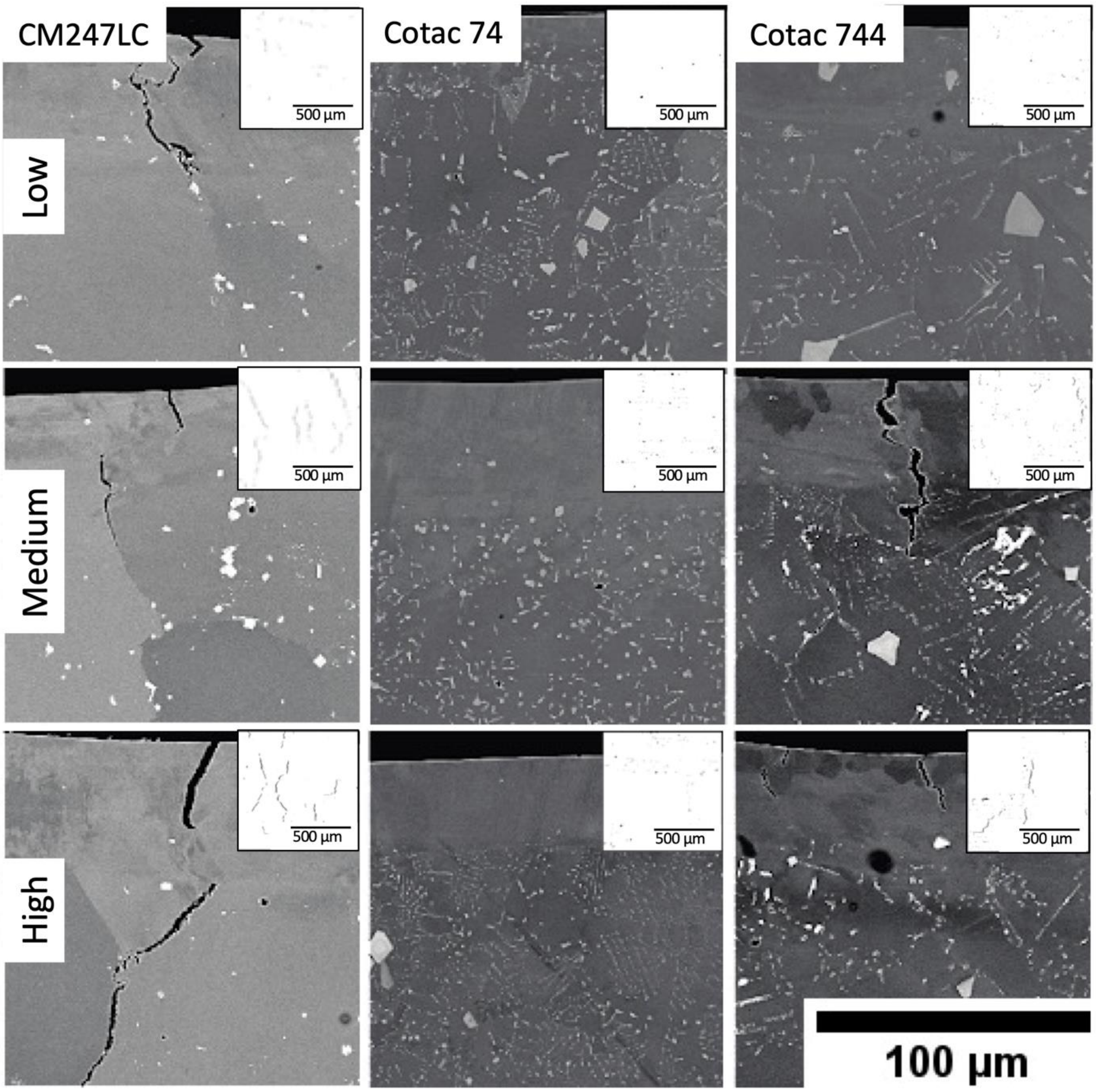

Figure 1 – SEM cross-section images of the as-cast alloys CM247LC, Cotac-74, and Cotac-744 following laser-pass assessment. Insets in each condition show a binary threshold image of the laser surface providing a clearer representation of the cracking severity in each condition. No cracks were observed for Cotac-74 for any of the three laser-pass conditions. Surface breaking cracks can be seen in all conditions for CM247LC, with cracking observed in the medium and high-power regimes for Cotac-744.

3.2 Thermodynamic Analysis

To determine the solidification ranges and the solvus temperatures of the γ′ phase for Cotac-74 and Cotac-744, DSC data were acquired from samples both in the as-built and as-cast state and compared against the equivalent conditions of CM247LC. The first heating curves of the alloys in the as-built state are shown in Figure 2. Table 2 summarises the key transition temperatures from all results in the as-cast and as-built states.

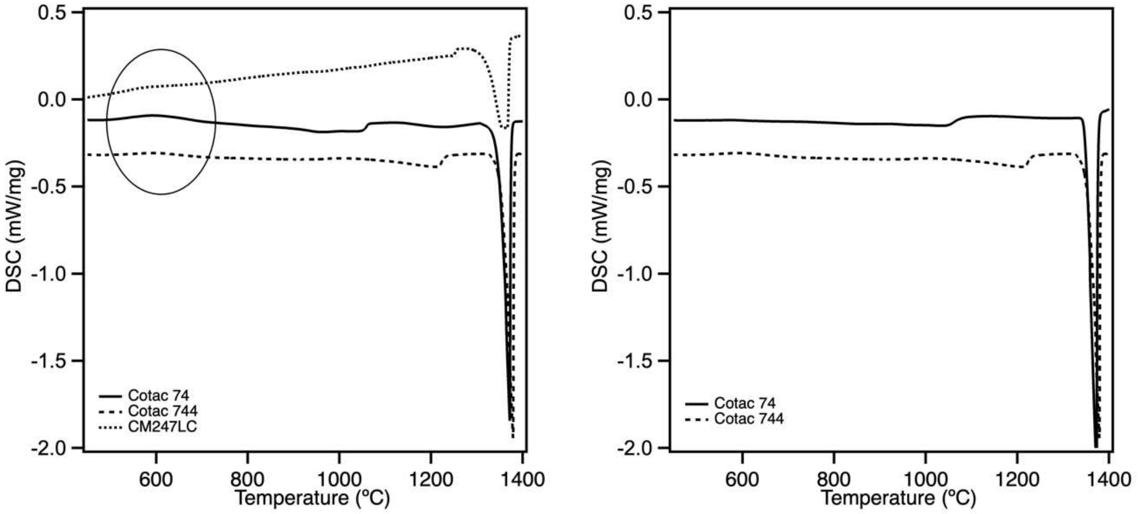

Figure 2 – Left: DSC first heating thermograms for the Cotac-74, Cotac-744 and CM247LC alloys in equivalent as-built conditions, Right: Equivalent DSC first heating thermograms of as-cast Cotac-74 and Cotac-744.

An exothermic event in the DSC heating data is present at approximately 500 – 700 °C for all as-built LPBF samples, but is notably absent in the as-cast samples. This event is commonly observed in AM processed superalloys and is thought to be associated with the precipitation of γ′ [3, 15]. On second heating, this event was no longer observed in any of the conditions, confirming that it is the result of a microstructural feature related to the LPBF processing.

Table 2 – Transition temperatures in degrees Celsius for the alloys used in this study, determined from analysis of the DSC data.

Thermal Events	CM247LC	Cotac-74		Cotac-744	
	LPBF	As-cast	LPBF	As-cast	LPBF
γ′ solvus – Mid Point	1251.5	1061	1059	1230	1226

Solidus Temperature	1279	1333	1303	1321	1320
Liquidus Temperature	1364	1340	1345	1353	1363
Approximate solidification range	85	7	42	32	45

The solidification range of each alloy was calculated from their respective liquidus temperature obtained on cooling and their solidus temperature obtained on heating. The values obtained for Cotac-744 in both conditions and for the as-built Cotac-74 are similar, although the value for as-cast Cotac-74 is unexpectedly low. The calculated solidification range for CM247LC is approximately double that of the Cotac alloys, with the narrower freezing range of these alloys being a result of the eutectic solidification behaviour, which is theorised to lead to improved hot cracking resistance [9-11].

The γ′ solvus temperature for all alloys is also reported in Table 2. Due to difficulties in determining the precise values of the onset and return to baseline, only the mid-point values corresponding to the point of maximum γ′ dissolution are reported. Cotac-744 is shown to have a significantly higher γ′ solvus temperature than Cotac-74 across both production routes and for all points of dissolution compared. This behaviour is to be expected due to the significantly higher Al content in Cotac-744 compared to Cotac-74 giving rise to both an increased γ′ solvus temperature as well as a higher γ′ volume fraction. The values for the solidus temperature and γ′ solvus obtained in the LPBF condition for both alloys were found to be in line with values reported in the literature [12, 14].

Of particular significance to assess the material for LPBF suitability is the temperature range of the alloys between the γ′ solvus and the solidus temperature. A larger temperature range is thought to be beneficial, reducing the cracking susceptibility of the material due to a reduction in the propensity for brittle, solute enriched films [16]. Based on the DSC thermograms obtained, this window is 20˚C for CM247LC, 230˚C for Cotac-74, and 80˚C for Cotac-744, further suggesting the possibility of a reduced cracking susceptibility for the Cotac alloys.

3.3 Microstructure and Cracking behaviour

Macroscopic images of the as-built samples of the Cotac alloys, Figure 3, revealed significant macrocracking and base delamination in both the Cotac-74 and Cotac-744 alloys following

LPBF processing. This was believed to be a result of non-optimised build parameters [17], as existing parameter sets commonly used for high γ' superalloys were chosen and no design of experiments studies were performed to enable parameter optimisation. Whilst the observed macrocracking is of concern, the results from the laser pass assessments suggest that microcracking can be reduced or eliminated in these materials, and therefore, processing optimisation may be feasible. Indeed, no microcraking was observed in samples of the Cotac-74 alloy, Figure 4, in either the as-built or solution-aged conditions. In contrast, solidification microcracks were visible throughout the microstructure of Cotac-744. This increased cracking susceptibility was consistent with the higher γ' content in Cotac-744 compared to Cotac-74, as well as the reduced temperature range between the terminus of γ' solvus and the solidus temperature.

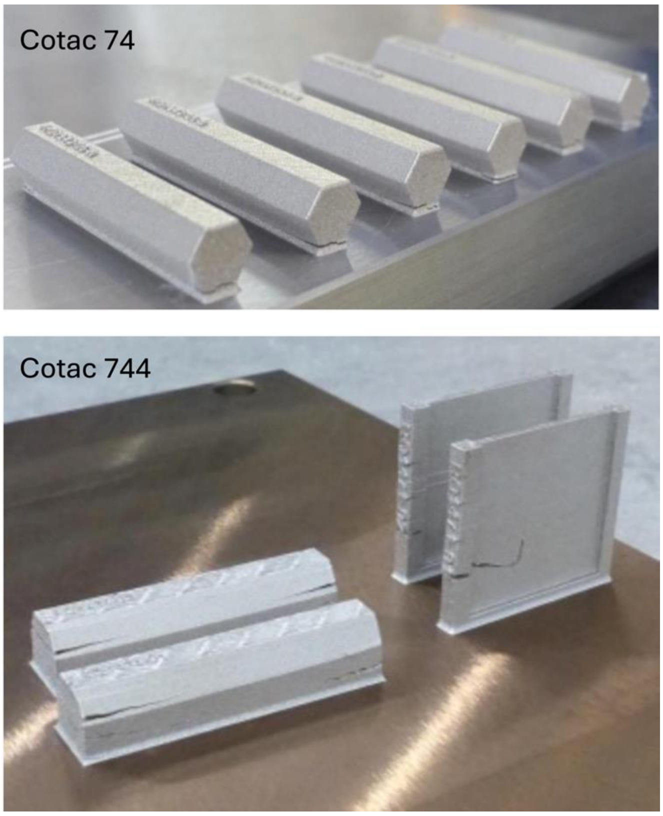

Figure 3 – Photographs of the Cotac-74 (top image) and Cotac-744 (bottom image) builds exhibiting macroscopic cracking behaviour and base delamination.

Figure 4 further reveals the microstructures of the alloys in the as-built states and following solution and ageing. In the as-cast state, both Cotac-74 and Cotac-744 alloys exhibited fine eutectically formed MC carbides, with larger, blocky MC precipitates also forming. Upon solution and ageing, the microstructure of Cotac-74 remained largely unchanged with only minor spheroidisation of a small fraction of the fine eutectic carbide network observed. In contrast, the eutectic carbide network in Cotac-744 was found to coarsen, with precipitation of bright phases, also believed to be carbides, occurring at high angle grain boundaries.

In contrast to the as-cast states, the as-built microstructures for both Cotac-74 and Cotac-744 were found to solidify with the typical cellular structure observed in LPBF and no evidence of the eutectic carbide networks. Instead, fine carbides were observed to form at cellular boundaries in both alloys. Following solution and ageing, these carbides persisted but additional coarse carbides were seen on the grain boundaries. Due to processing through LPBF, the γ' precipitates were fine in both alloys, however larger precipitates were observed in Cotac-744 due to the higher γ' content.

Examination of the as-built Cotac-74 microstructure produced via LPBF revealed a network of fine carbides. After heat treatment the carbide network remained, with coarser precipitates present. These were located primarily on the grain boundaries with a small amount of additional intragranular precipitation. As in Cotac-74, a fine MC carbide network was seen in the as-built material of Cotac-744. Following solution heat treatment and ageing these persisted but additional coarse carbides were seen on the grain boundaries. The formation of γ' precipitates was also observed following solution and ageing, with significantly finer γ' particles observed in Cotac-74 compared to Cotac-744.

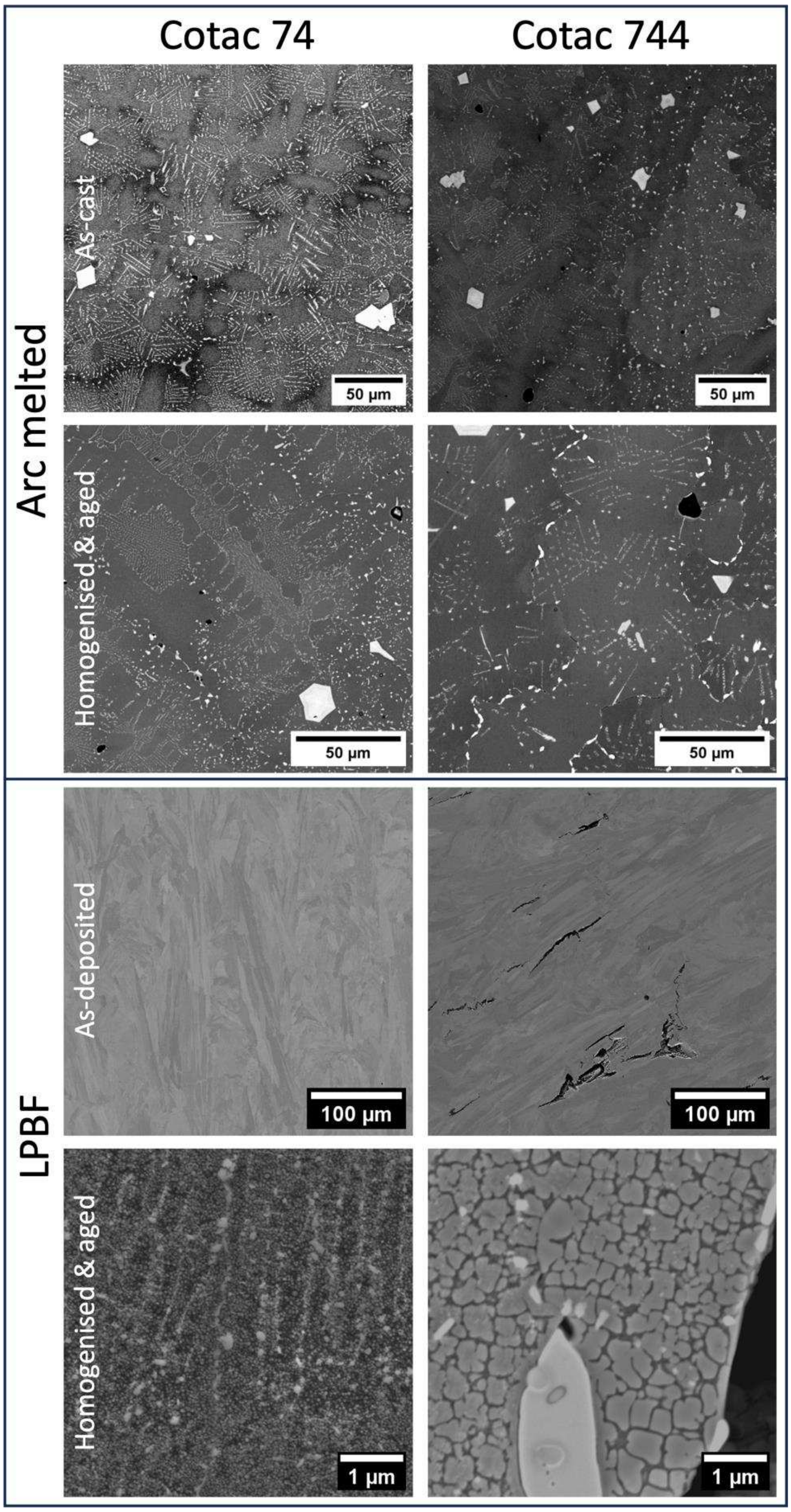

Figure 4 – Backscattered electron micrographs for Cotac-74 and Cotac-744 produced by arc melting and LPBF in the as-built states and following solution heat treatment and ageing.

3.4 Phase Analysis

To further explore the microstructures of the Cotac alloys following LPBF, as well as determine the crystallographic nature and elemental constitution of the precipitating phases, XRD and TEM analyses were performed. Figure 5 summarises the XRD results obtained whereas Figures 6 and 7 show STEM-EDX maps and selected area diffraction patterns (SADPs) from the key phases from the solution and aged states.

Examination of the XRD data obtained from the LPBF material revealed the presence of γ/γ' fundamental peaks and MC carbide peaks in the as-built condition for both alloys. The associated lattice parameters of the phases obtained through Pawley refinements are shown in Table 3. Due to the absence of superlattice γ' peaks, the difficulty in clearly separating distinct γ and γ' contributions in the fundamental peaks, as well as the generally accepted theory of the absence of γ' formation in the as-built condition for superalloys, only the lattice parameters for the γ and MC carbide phases could be obtained for the as-built state.

As expected, for both Cotac alloys, peaks associated with MC carbides were observed in the XRD traces. Based on the compositions of the alloys, these carbides should be nearly pure NbC, as Nb is the only strong MC carbide former in both alloys. However, comparing the lattice parameters obtained in the as-built state to that of pure NbC, which has a lattice parameter of 4.470 Å [18], it is clear that Nb is not the only metal conjugate in the carbides formed.

Following solution and ageing, the XRD results obtained differed for the two alloys. For Cotac-74, no additional peaks were observed that would indicate the presence of additional phases. However, the MC carbide peaks were seen to split into doublets suggesting the potential formation of carbides with distinct compositions. This phenomenon was previously reported by Divya *et al.* [19] and was believed to be due to the formation of non-equilibrium MC species during the LPBF processing. Analysis of the lattice parameters of these carbides suggests that one of the MC species approaches pure NbC, with the second species exhibiting a smaller lattice parameter. The STEM-EDX analysis revealed the presence of both large and small carbides rich in Nb. It is believed that the larger, more Nb-rich carbides formed from the eutectic MC carbide particles, with more compositionally-complex finer carbides precipitating during the subsequent ageing. In addition to the MC carbides, and despite no additional peaks identified in the XRD patterns, STEM-EDX of the solution and aged Cotac-74 alloy indicated the formation of strongly Cr-rich carbides, believed to be $M_{23}C_6$. Crystallographic confirmation of the presence of $M_{23}C_6$ was obtained through electron diffraction, which further revealed a [0 0 1]//[0 0 1] orientation relationship between the $M_{23}C_6$ and γ phase. From the literature, it was reported by Khan *et al.* [12] that this phase evolves from the transformation of MC at temperatures in the range of 700 to 1000 °C, consistent with the ageing temperature of Cotac-74.

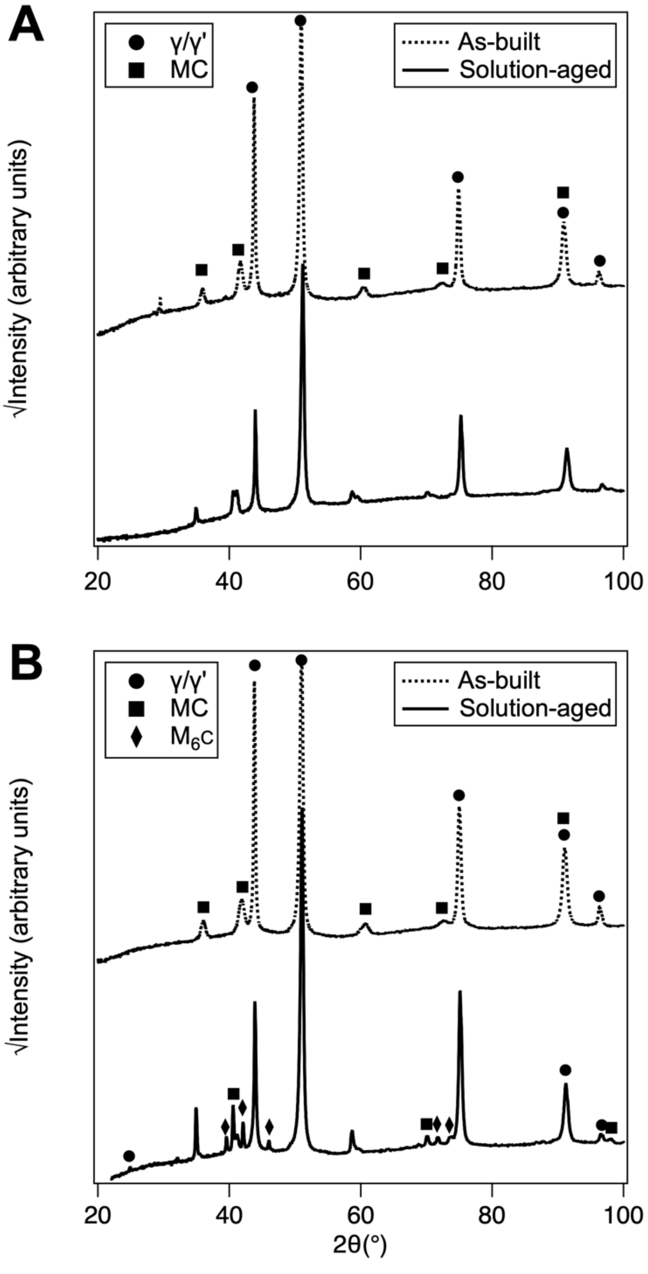

Figure 5 – XRD traces for Cotac-74 (A) and Cotac-744 (B) in the as-built and solution-aged conditions. Note the split MC peaks in the solution-aged condition.

Table 3 – Lattice parameters of the phases in Cotac-74 and Cotac-744, determined through Pawley refinement of

the XRD data.

	Cotac-74		Cotac-744	
Lattice Parameter / Å	As-built	Solution-aged	As-built	Solution-aged
γ	3.580	3.573	3.577	3.573
γ'	-	3.585	-	3.586
MC Carbide – 1	4.332	4.441	4.316	4.437
MC Carbide - 2	-	4.393	-	4.384
M_6C	-	-	-	11.151

Similarly to Cotac-74, the MC carbide peaks in the XRD patterns for Cotac-744 following solution and ageing also showed splitting, enabling two distinct MC species to be identified; one closer to pure NbC, and the other exhibiting a smaller lattice parameter. However, in contrast to Cotac-74, the XRD patterns from the solution and aged Cotac-744 did also show additional peaks not resulting from the γ/γ' and MC phases. These additional peaks were identified to be due to the formation of the M_6C phase, which was also confirmed through electron diffraction, Figure 7. The formation of the M_6C phase instead of the $M_{23}C_6$ phase was believed to be due to the lower content of Cr and higher content of Mo in Cotac-744 compared to Cotac-74 [12].

From STEM-EDX data, the M_6C phase was found to be rich in Mo and W. Though the M_6C was not identified by Khan *et al.* [12], it was observed by Kachanov *et al.* [20] and Petrushin *et al.* [21] in alloys with a similar composition. It was posited that this phase can form in preference to $M_{23}C_6$ from the reaction of the γ and MC carbides at higher temperature. This may arise as a result of the solidification induced microsegregation associated with LPBF processing and may be further influenced by subsequent heat-treatments applied. It is therefore likely that correct optimisation of heat-treatments specific to LPBF may be required to avoid the occurrence of M_6C.

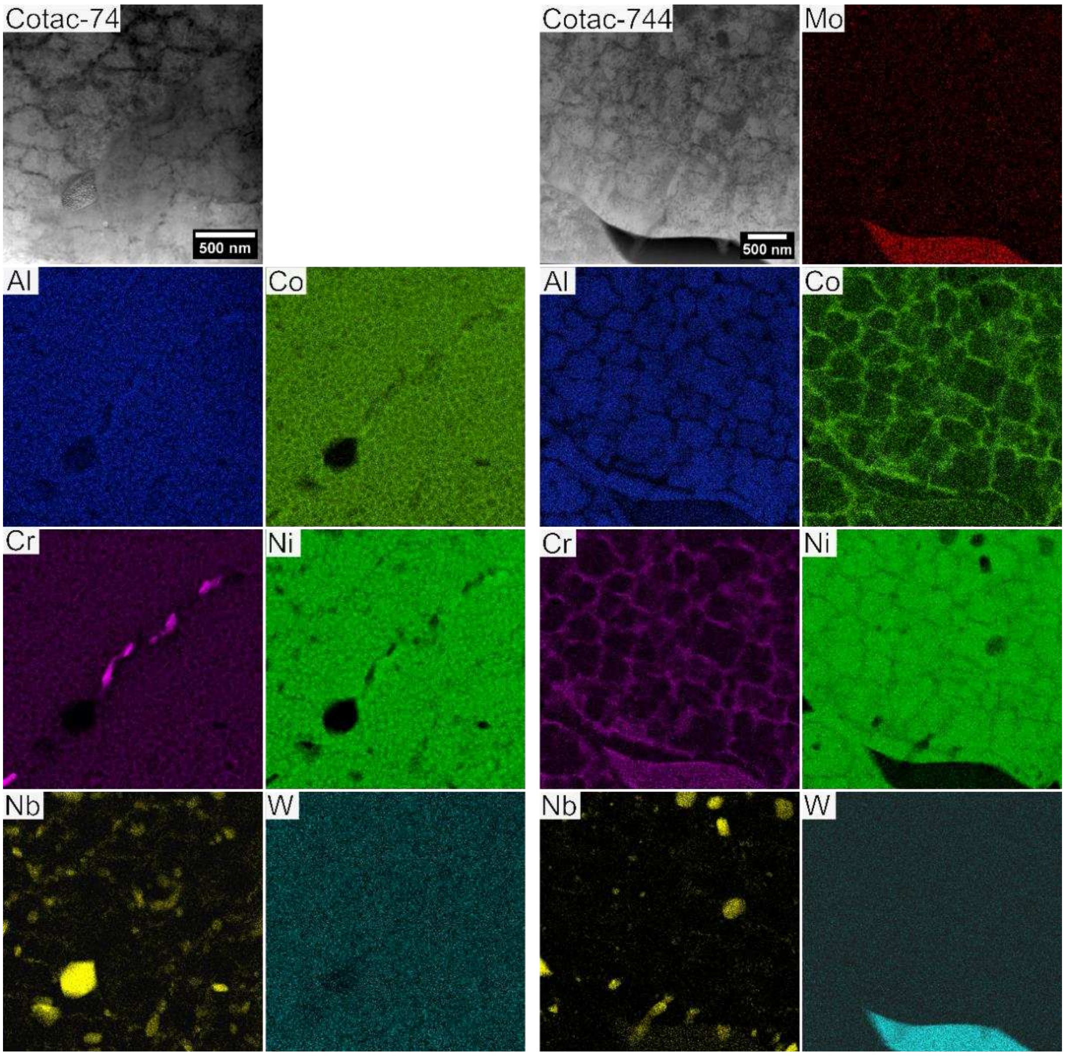

Figure 6 – STEM-EDX analysis of solution-aged Cotac-74 and Cotac744. In each instance, the first image is a bright field electron micrograph. Individual elemental concentration maps have been provided for each of the major elements in the alloys.

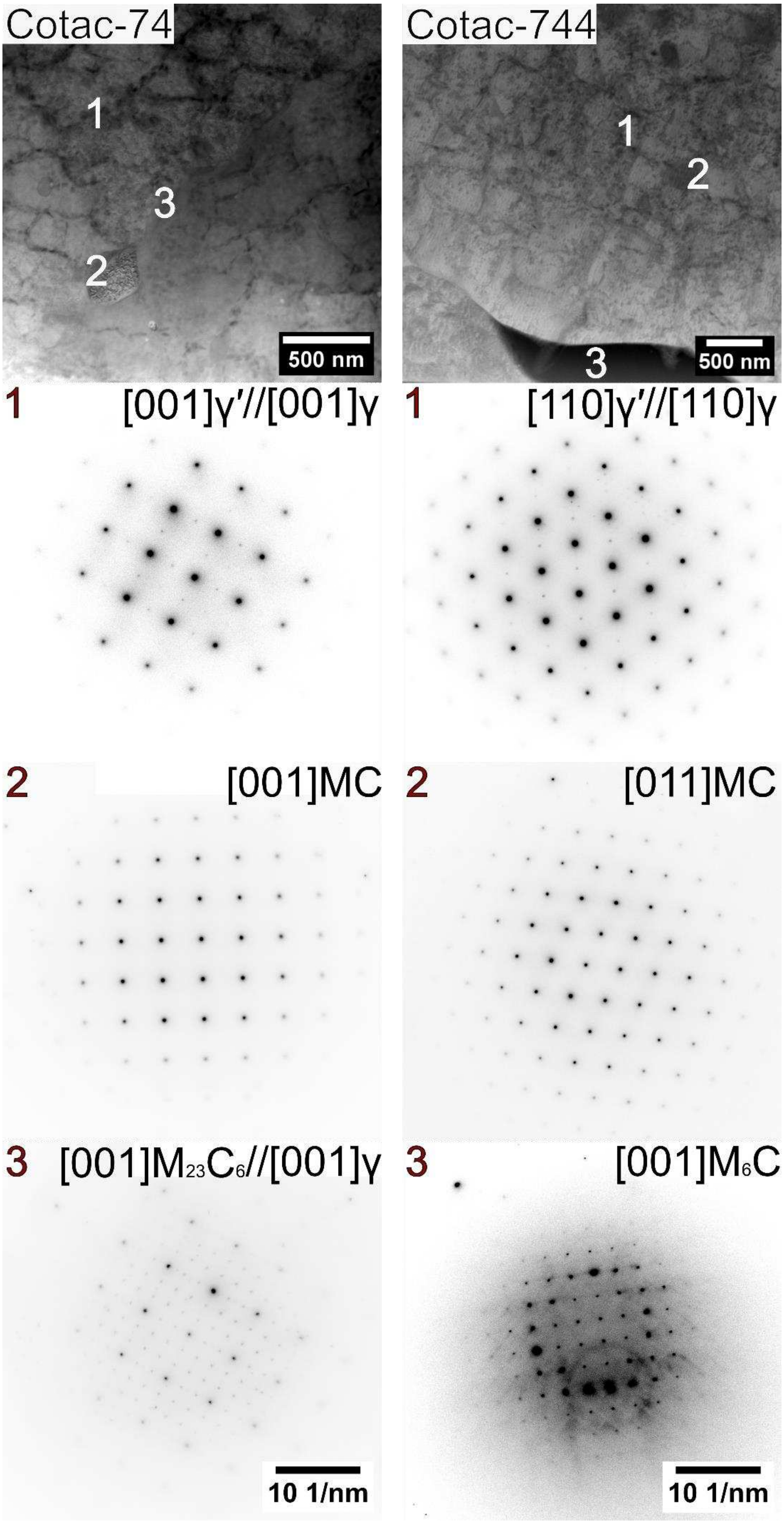
Cotac-74
1
3
2
500 nm
Cotac-744
1
2
3
500 nm
1 [001]γ′//[001]γ
1 [110]γ′//[110]γ
2 [001]MC
2 [011]MC
3 [001]M23C6//[001]γ
3 [001]M6C
10 1/nm
10 1/nm

Figure 7 – TEM analysis of the solution-aged Cotac-74 and Cotac744. In each instance, the first image is a bright field electron micrograph with numbered regions. The number corresponds to the regions where SADPs were taken from. The specific SADPs have been provided below the bright field micrographs for each alloy. For each SADPs the orientation and, if relevant, the orientation relationship have been provided. Due to the textured nature of the samples it was not always possible to orient the cubic phases along the [100] planes. In both alloys the γ′ superlattice reflections are visible in the SADPs.

Conclusions

The results presented in this study highlight the potential advantage of using the γ-γ′-MC eutectic superalloys for additive manufacturing. Both eutectic Cotac alloys studied herein displayed increased cracking resistance in the laser-pass assessment when compared to CM247LC. Indeed, Cotac-74 displayed no microcracking when processed through LPBF. In addition, no deleterious or unexpected phases were detected in the Cotac-74 alloy following processing through LPBF in either the as-built or heat-treated conditions. However, further exploration of the process parameters and part geometry is required to eliminate the macro-cracking and realise the increased temperature capability of these alloys above other crack-free LPBF Ni-based superalloys. Additional research into the development of these non-traditional Ni-based superalloys for additive manufacturing processing is therefore warranted.

Acknowledgements

The authors acknowledge funding and in-kind support from Rolls-Royce plc. Assistance in the preparation and processing of samples by Mrs. Sue Rhodes is gratefully acknowledged. The authors would like to acknowledge the work of Geoff West at the University of Warwick in the preparation of FIB samples for the TEM work completed. Experimental access to TEM facilities was supported by the Henry Royce Institute through EPSRC Grants EP/ R00661X/1, EP/S019367/1, EP/P025021/1 and EP/ P025498/1.

References

[1] B. Kappes, S. Moorthy, D. Drake, H. Geerlings, A. Stebner, Machine Learning to Optimize Additive Manufacturing Parameters for Laser Powder Bed Fusion of Inconel 718, 9th International Symposium on Superalloy 718 & Derivatives: Energy, Aerospace, and Industrial Applications., Springer International Publishing, Pittsburgh, 2018.

[2] K.A. Christofidou, H.T. Pang, W. Li, Y. Pardhi, C.N. Jones, N.G. Jones, H.J. Stone, Microstructural Control and Optimization of Haynes 272 Manufactured Through Laser Powder Bed Fusion, in: S. Tin (Ed.) Superalloys 2020, 2020.

[3] J.F.S. Markanday, K.A. Christofidou, J.R. Miller, E.R. Livera, N.G. Jones, E.J. Pickering, W. Li, Y. Pardhi, C.N. Jones, H.J. Stone, The Microstructural Evolution of CM247LC Manufactured Through Laser Powder Bed Fusion, Metallurgical and Materials Transactions A (2023).

[4] J.H. Boswell, D. Clark, W. Li, M.M. Attallah, Cracking during thermal post-processing of laser powder bed fabricated CM247LC Ni-superalloy, Materials & Design 174 (2019).

[5] J.F.S. Markanday, Applications of alloy design to cracking resistance of additively manufactured Ni-based alloys, Materials Science and Technology (2022) 1-15.

[6] I. Baturynska, O. Semeniuta, K. Martinsen, Optimization of Process Parameters for Powder Bed Fusion Additive Manufacturing by Combination of Machine Learning and Finite Element Method: A Conceptual Framework, Procedia CIRP 67 (2018) 227-232.

[7] Z. Sun, Y. Ma, D. Ponge, S. Zaefferer, E.A. Jagle, B. Gault, A.D. Rollett, D. Raabe, Thermodynamics-guided alloy and process design for additive manufacturing, Nat Commun 13(1) (2022) 4361.

[8] J.N. Ghoussoub, S. Utada, F. Pedraza, W.J.B. Dick-Cleland, Y.T. Tang, R.C. Reed, Alloy Design for Additive Manufacturing: Early-Stage Oxidation of Nickel-Based Superalloys, Metallurgical and Materials Transactions A 54(5) (2022) 1721-1729.

[9] Y.T. Tang, C. Panwisawas, J.N. Ghoussoub, Y. Gong, J.W.G. Clark, A.A.N. Németh, D.G. McCartney, R.C. Reed, Alloys-by-design: Application to new superalloys for additive manufacturing, Acta Materialia 202 (2021) 417-436.

[10] S. Kou, A criterion for cracking during solidification, Acta Materialia 88 (2015) 366-374.

[11] L. Chechik, K.A. Christofidou, L. Farquhar, M. Tse, G. Baxter, I. Todd, Tools for the Assessment of the Laser Printability of Nickel Superalloys, Metallurgical and Materials Transactions A 54(6) (2023) 2421-2437.

[12] T. Khan, J.F. Stohr, H. Bibring, COTAC 744: An optimised D.S. composite for turbine blades, Superalloys 1980, TMS, 1980, pp. 531-540.

[13] N. Zhou, A.D. Dicus, S.A. Forsik, T. Wang, G.A. Colombo, M.E. Epler, Development of a new alumina-forming crack-resistant high-γ' fraction Ni-base superalloy for additive manufacturing, Superalloys 2020, 2020.

[14] H. Bibring, T. Khan, M. Rabinovitch, J.F. Stohr, Development and evaluation of new industrial DS monocarbide reinforced composites for turbine blades, Superalloys 1976, Seven Springs, PA, 1976, pp. 331-340.

[15] O.M.D.M. Messé, R. Muñoz-Moreno, T. Illston, S. Baker, H.J. Stone, Metastable carbides and their impact on recrystallisation in IN738LC processed by selective laser melting, Additive Manufacturing 22 (2018) 394-404.

[16] S.P. Murray, K.M. Pusch, A.T. Polonsky, C.J. Torbet, G.G.E. Seward, N. Zhou, S.A.J. Forsik, P. Nandwana, M.M. Kirka, R.R. Dehoff, W.E. Slye, T.M. Pollock, A defect-resistant Co-Ni superalloy for 3D printing, Nat Commun 11(1) (2020) 4975.

[17] A. Jena, S.E. Atabay, A. Gontcharov, P. Lowden, M. Brochu, Laser powder bed fusion of a new high gamma prime Ni-based superalloy with improved weldability, Materials & Design

208 (2021).

[18] E.K. Storms, N.H. Krikorian, The Variation of Lattice Parameter with Carbon Content of Niobium Carbide, Journal of Physical Chemistry 63(10) (1959) 1747-1749.

[19] V.D. Divya, R. Muñoz-Moreno, O.M.D.M. Messé, J.S. Barnard, S. Baker, T. Illston, H.J. Stone, Microstructure of selective laser melted CM247LC nickel-based superalloy and its evolution through heat treatment, Materials Characterization 114 (2016) 62-74.

[20] E.B. Kachanov, N.V. Petrushin, I.L. Svetlov, Heat-resistant eutectic alloys with carbide-intermetallic strengthening, Metal Science and Heat Treatment 37(3-4) (1995) 154-159.

[21] N.V. Petrushin, E.M. Visik, M.A. Gorbovets, R.M. Nazarkin, Structure–phase characteristics and the mechanical properties of single-crystal nickel-based rhenium-containing superalloys with carbide–intermetallic hardening, Russian Metallurgy (Metally) 2016(7) (2016) 630-641.